Carbohydrate Polymers 157 (2017) 1013–1023

Contents lists available at ScienceDirect

Carbohydrate Polymers

journal homepage: www.elsevier.com/locate/carbpol

Resistant starch/pectin free-standing films reinforced with nanocellulose intended for colonic methotrexate release

Andréia B. Meneguin[a,d,*], Beatriz Stringhetti Ferreira Cury[b], Aline M. dos Santos[b], Douglas Faza Franco[c], Hernane S. Barud[c,d], Edson C. da Silva Filho[a]

[a] Interdisciplinary Laboratory of Advanced Materials, Centro de Ciências da Natureza – CNN, Universidade Federal do Piauí – UFPI, 64049-550 Teresina, PI, Brazil
[b] Department of Drugs and Pharmaceuticals, Faculty of Pharmaceutical Sciences, São Paulo State University-UNESP, 14800-903 Araraquara, SP, Brazil
[c] Institute of Chemistry, São Paulo State University – UNESP, 14801-970 Araraquara, SP, Brazil
[d] Universidade de Araraquara – UNIARA, 14801-320 Araraquara, SP, Brazil

ARTICLE INFO

Article history:
Received 15 July 2016
Received in revised form 19 October 2016
Accepted 20 October 2016
Available online 21 October 2016

Keywords:
Nanocellulose
Cellulose nanofiber
Resistant starch
Pectin
Free-standing films
Methotrexate

ABSTRACT

Although resistant starch/pectin (RS/P) films have previously displayed suitable properties for colon-specific drug delivery, nanocomposite films were developed aiming to enhance physicochemical, thermal, mechanical and barrier properties, as well as the low oral bioavailability of methotrexate (MTX). *FEG-SEM* micrographs of nanocomposite films showed different interaction patterns occurring among nanocellulose and RS/P. The nanofiller addition led to an increase in the thermal stability, probably due to its interaction with RS crystalline double helices. Results also displayed an improvement of the puncture strength, while barrier properties revealed a low water vapor permeability. *Ex vivo* bioadhesion test displayed the nanocomposites films to interact strongly with porcine gastrointestinal mucosa. *In vitro* drug release studies showed that the films developed enhanced the drug dissolution rates with approximately 80% of MTX release in 150 min, suggesting the potential of these materials as a poor solubility drugs carrier, which constitutes an important tool for enhancing oral bioavailability.

1. Introduction

The development of materials aiming colon-specific drug delivery have been the subject of many researches in the last years due mainly to the fast development and approbation of new therapeutic proteins by FDA (Koetting, Guido, Gupta, Zhang, & Peppas, 2016), and the uncontrolled emergence of new bowel inflammatory diseases, such as ulcerative colitis and Chron's disease, as well as colorectal cancer (Maurer et al., 2016).

Regarding proteins, some properties of the colon, such as the reduced proteolytic activity, the prolonged transit time and the pH near to neutrality make it as a promising site for release and/or absorption of therapeutic proteins/peptides. Moreover, the local release of intestinal anti-inflammatory and anticancer agents should allow the improvement of therapeutic effect, avoiding important side effects (He, Du, Cao, Xiang, & Fan, 2008; Maurer et al., 2016).

Films coating intended to colonic drug delivery can be based on materials that are specifically degraded by enzymes produced by colonic bacteria such as resistant starch (RS). The RS is a hydrothermally modified starch that escapes from digestion in the upper GIT portions, due mainly to its three-dimensional structure more packaged and in the form of double helices stabilized by hydrogen bonds (Meneguin, Cury, & Evangelista, 2014). Pectin (P) is a natural heteropolysaccharide found in different plant species that also plays an important role for targeting drugs to the colon, since it is resistant to amylases and proteases digestion, and it remains as a macromolecular aggregate when in acid medium. Likewise, it is biodegradable, biocompatible and nontoxic (Cury, Meneguin, Cardoso, & Prezotti, 2014).

In a recent paper published by some of us (Meneguin et al., 2014), free-standing films of RS/P blends were developed and their mechanical (puncture resistance and elongation at break), swelling and barrier (water vapor permeability) properties demonstrated that these mixtures allowed to obtain materials with suitable fil-

* Corresponding author at: Interdisciplinary Laboratory of Advanced Materials, Centro de Ciências da Natureza – CNN, Universidade Federal do Piauí – UFPI, 64049-550 Teresina, PI, Brazil.
E-mail addresses: abagliottim@hotmail.com (A.B. Meneguin), curybsf@fcfar.unesp.br (B.S. Ferreira Cury), aline.martinsdossantos@yahoo.com.br (A.M. dos Santos), fazafranco@yahoo.com.br (D.F. Franco), hernane.barud@gmail.com (H.S. Barud), edsonfilho@ufpi.edu.br (E.C. da Silva Filho).

http://dx.doi.org/10.1016/j.carbpol.2016.10.062
0144-8617/

mogenic properties. These films also presented promising features to achieve colon-specific drug delivery, such as high RS contents (65.80–96.69%) and resistance against enzymatic digestion in upper portions of GIT.

However, films based on natural polymers present inherent disadvantages, such as high water solubility that can often lead to a premature release of the drug (He et al., 2008; Liu, Fishman, Kost, & Hicks, 2003). In this sense, the development of nanocomposites by the reinforcement of a polymer matrix with a nano-scale filler (Rhim, 2011) represents a simple and rational strategy to overcome this problem. This happens because the homogeneous dispersion of the nanocomposite distinct phases can provide different and improved properties in comparison to isolated materials, such as enhanced mechanical, barrier and thermal properties (Saha et al., 2016).

Nanocellulose – a promising biopolymer for designing nanocomposite drug delivery systems – has received much attention in the medical and pharmaceutical field, since the nanofiller provides strong polymer-filler interactions due to its large surface area, reason why small amounts of reinforcement enhance significantly the material properties (Mandal & Chakrabarty, 2015). In fact, nanocellulose is a product that has nanoscale structures, showing excellent mechanical, barrier, nanoreinforcement and biological properties, mainly because of its high crystallinity. It is important to highlight that the three hydroxyl-groups present in each individual glucose unit originate a highly reactive structure, which allows interaction with other molecules or with enzymes and/or proteins (Lin & Dufresne, 2014).

The three existing different types of nanocellulose are listed as follows. The first one, bacterial cellulose (BC), corresponds to an exopolysaccharide produced from bacteria, which displays a reduced size (20–100 nm), and an increased number of fibrils. The second one, the cellulose nanocrystals (CNC or cellulose nanowhiskers), has a diameter between 5 and 30 nm and length of 100–500 nm, and is obtained by chemical processes, such as acid hydrolysis of plant cellulose, in which amorphous structures are removed, preserving only the crystalline portion. At least, the third one, the cellulose nanofibrils (CNF), consists of individual and aggregate nanofibers of 1 μm length and 10–100 nm diameter obtained by grinding or in a high-pressure homogenizer due to the exfoliation (Kim et al., 2015) of interfibrillar hydrogen bonds (Abeer, Iqbal, & Martin, 2014; Jorfi & Foster, 2015). According to Eichhorn et al. (2010), CNF has been reported as one of the best biopolymer reinforcement due to its specific stiffness.

Qiao et al. (2015) carried out experiments with composite hydrogels based on BC nanofibers (BCN) and poly (vinyl alcohol) (PVA) for medical (artificial cartilage and blood vessel) and pharmaceutical applications (drug delivery systems). The authors demonstrate that the BCN acts as a crosslinker agent, leading to the construction of more organized and compact porous structures due to hydrogen bonding interaction between PVA groups and nanofibers, in addition to the physical crosslinking. Moreover, because of the uniform distribution between the hydrophilic matrix and reinforcement phases, as well as the high Young's modulus and strength, BCN was responsible to enhance mechanical properties, thus the modulus increased 97.4% in relation to pure PVA.

Another paper, presented by Juncu, Stoica-Guzun, Stroescu, Isopencu, and Jinga (2015), reported the preparation of BC/Carboxymethylcellulose (CMC) composite films crosslinked with citric acid aimed the controlled release of ibuprofen. They found that when BC was at the lowest concentration, the swelling and drug release rates were increased in relation to CMC film, which was attributed to the raising of hydrophilicity in the system. However, such swelling and drug release rates could be effectively controlled by increasing the concentration of BC in the nanocomposite, because of a wider crosslinked polymer network from the reaction of numerous hydroxyl groups with citric acid.

Hence, the investigation of cellulose nanofibers addition as a reinforcement material to build nanocomposite films based on RS/P as a colon-specific drug delivery system was evaluated. Methotrexate (MTX), a poorly water-soluble drug, with important therapeutic effects in the treatment of bowel inflammatory disease, such as ulcerative colitis and Chron's disease, and colorectal cancer was used as model drug. Nanocomposite films structural, morphological, thermal, mechanical, mucoadhesive and barrier properties were analyzed, along with the ability to control the drug release rates.

2. Materials and methods

2.1. Materials

Concerning the materials used during the processes documented in the following pages, at first, high amylose starch – HAS (type Hylon VII – 68% amylose, lot:HA9140), which was a gift from the National Starch & Chemical (New Jersey, EUA). Second, cellulose nanofibrils (CNF) at 1.4% (w/w), obtained by grinding of plant cellulose, that were provided by Suzano Papel e Celulose, Brazil. Third, pectin (type LM-5206CS – DE < 50%, lot: S74431) was granted by CP Kelco (Copenhagen, Dinamarca). At least, glycerin (99.5%, lot: 0807381), which was purchased from Vetec (Duque de Caxias, Brazil).

2.2. Methods

2.2.1. BC membranes preparation

BC membranes were produced according to Barud et al. (2015). Briefly, cultures of *Gluconacetobacter hansenii* (strain ATCC 23769) were incubated for 96 h at 28 °C in trays 30 cm × 50 cm, using a static Hestrin and Schramm (HS) culture medium. It was composed by 50 g/L glucose, 4 g/L of yeast extract, 0.73 g/L of $MgSO_4 \cdot 7H_2O$, 2 g/L KH_2PO_4, 20 g/L ethanol and distilled water. Then, all BC membranes obtained were washed several times in water, until neutral pH, with 1 wt% aqueous NaOH at 70 °C in order to remove bacteria.

2.2.2. Production of BC nanofibers (BCN) suspension

A suspension of BCN at 2.33% (w/v) was obtained by shearing wet BC membranes (25 cm^2) in an ultra-turrax high energy disperser IKA® (T18 model) at 13000 rpm for 1 h with the addition of 400 mL of water. After this, the dispersions were centrifuged at 2000 rpm for 10 min and the supernatant was discarded.

2.2.3. HAS retrogradation associated to pectin

A hydrothermal process was applied to the HAS retrogradation according to Meneguin, Cury and Evangelista (2014). Briefly, HAS aqueous dispersion (5%) was autoclaved at 121 °C (120 min) for starch gelatinization, followed by its mixture with aqueous pectin dispersion (5%) at 1:1 ratio. Then, the gelatinized starch/pectin dispersion was submitted to thermal cycles alternating of 4 °C and 30 °C during 16 days (2 days at each temperature).

2.2.4. Preparation of nanocomposite films

The technique to prepare the nanocomposite films, based on RS/P and reinforced with cellulose nanofibers is illustrated in Fig. 1A. Different concentrations (0.5, 1.0, 2.0 and 3.0%, *w/w*) of BCN or CNF were added to the RS/P dispersions obtained in section 2.2.3. Next, glycerin was added at 5% (*w/v*) in relation to dry polymer mass as plasticizer. Dispersions were kept under magnetic stirring (750 rpm) for 120 min to complete homogenization. A pre-determined volume of these dispersions (0.20 mL cm^{-2}) was poured into a Petri dish and dried in an oven-dryer at 40 °C

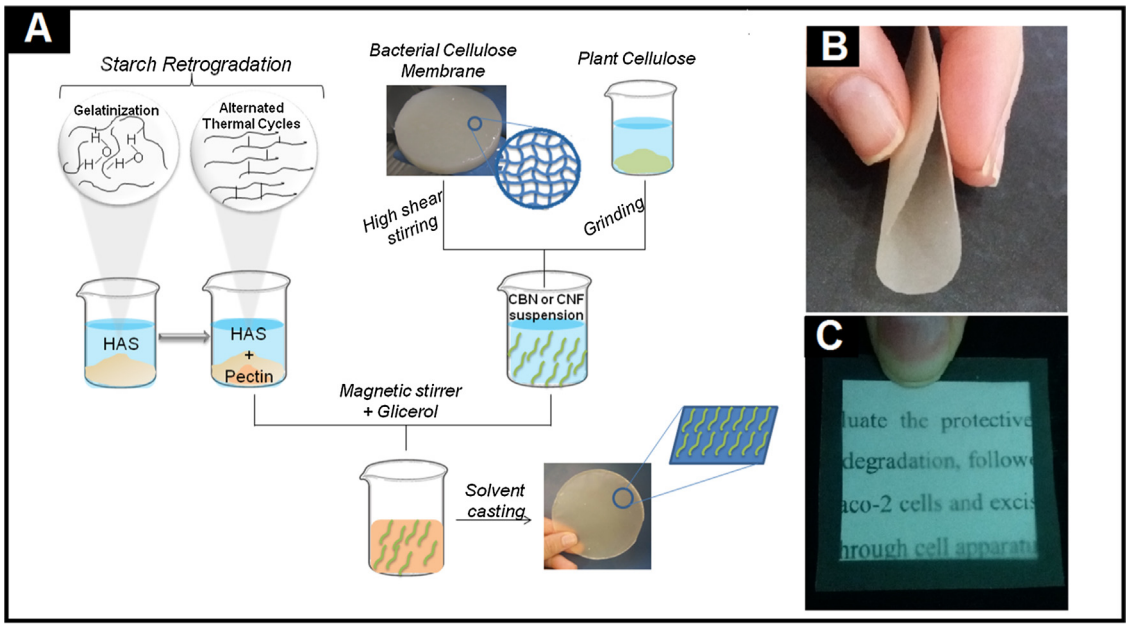

Fig. 1. Schematic illustration of the nanocomposite films preparation technique (A) and images of a representative nanocomposite film demonstrating its high flexibility (B) and transparence (C).

overnight. The following steps consisted in peeling the films from the Petri dish and keeping them for subsequent studies in a desiccator containing silica gel. Films without cellulose nanofibers were also prepared as a control sample.

Samples were labeled according to the type of nanofiber (BCN or CNF) added to the RS/P control film and its concentration (0.5, 1.0, 2.0 or 3.0%), as follows: RS/P-0.5BCN, RS/P-1.0BCN, RS/P-2.0BCN, RS/P-3.0BCN, RS/P-0.5CNF, RS/P-1.0CNF, RS/P-2.0CNF and RS/P-3.0CNF.

2.2.5. Macroscopic observations and thickness analysis

Control and nanocomposite films were macroscopically evaluated by considering flexibility, transparence and bubbles or fissures presence. The thickness of film samples was accurately measured with the digital micrometer MDC-Lite (Mitutoyo®) in five random positions. The analysis were made in sextuplicate and the average values were used in the mechanical properties calculations.

2.2.6. Field emission gum scanning electron microscopy (FEG-SEM)

Through FEG- SEM (JEOL JSM-7500F), it was possible to evaluate surface and transversal sections morphology of control and nanocomposite films. The film surface photomicrographs were taken at magnification, while cross-sections were registered at 1000 and 15,000× magnification. The films were attached to slab surfaces with double sided adhesive tape and then coated with a layer of carbon. Films were cryofractured by their immersion in liquid nitrogen aiming cross-section observations. All samples were examined using an accelerating voltage of 10 kV.

2.2.7. FTIR spectroscopy

FTIR spectra of pectin, resistant starch, BCN, CNF, RS/P-3.0BCN and RS/P3.-CNF representative samples were measure using a Perkin Elmer Spectrum 100 spectrometer in ATR mode. The spectra were collected over the range of 4000–600 cm^{-1} with an accumulation of 16 scans, resolution of 4 cm^{-1} and interval of 0.5 cm^{-1}.

2.2.8. TG/DTG

TG/DTG analysis were performed *via* a TA SDT 2960 (TA Instruments, USA) at a heating rate of 10 °C/min, from 25 to 500 °C, under nitrogen atmosphere (flow rate of 50 mL/min), in open aluminum pans containing about 7 mg of sample.

2.2.9. XRD

The X-ray diffraction analysis of pristine polymers, control (RS/P) and representative nanocomposite films (RS/P-3.0BCN and RS/P-3.0CN) were performed on a X-ray diffractometer (Siemens® – Model D5000; Germany), using nickel filtered CuKα radiation (λ = 1.5406 Å) (tube operating at 40 kV and 30 mA). Scanning regions were collected between 4 and 60° (2θ) in step size of 0.05° (2θ).

2.2.10. Mechanical properties analysis

The mechanical properties of control and nanocomposite films were evaluated on a Texture analyzer TA-XT2 (Stable Micro Systems), using a spherical-ended puncture probe (5 mm). The film sections were fixed on a metallic holder with a circular hole (D = 10 mm) and the probe was moved down at 1 mm s^{-1}. During the test, the velocity was constant (0.1 mm s^{-1}). The trigger force was 0.005 kg and force *versus* displacement curves recorded until the film rupture were used to determine the puncture strength (P_s), elongation at break (E_b) and perforation energy (E_p) parameters, according to the following equations (Eqs. (1)–(3)) (Limmatvapirat, Limmatvapirat, Puttipipatkhachorn, Nuntanid, & Luangtana-Anan, 2007; Meneguin et al., 2014):

$$Ps = \frac{F}{A} \quad (1)$$

where F (N) is the force required to fracture the film, and A (m^2) is the sectional area of the film ($A = 2rh$, in which r is the hole radius and h is the film thickness).

$$E_b = \frac{\sqrt{r^2 + d^2} - r}{r} \times 100 \quad (2)$$

Specifying r (mm) as the exposed film radius on the orifice plate and d as the displacement.

$$E_p = \frac{AUC}{V} \quad (2)$$

Finally, *AUC* means the area under curve force *versus* displacement, and V is the film volume ($V = \pi r^2 h$, in which r is the hole radius and h is the film thickness) placed on the orifice plate.

2.2.11. Water vapor permeability (WVP)

Circular sections of control and nanocomposite films were fixed on the top of glass cups (1.1 cm opening) containing 10 mL of water (100% *RH* gradient at 25 °C). The set was accurately weighed and stored in a desiccator containing silica gel (0% RH). The *RH* inside the cell was always higher than in the outside, and the water vapor transport was determined from the cup weight loss. The changes about the cup weight were plotted as a time function (24, 48, 72, 96 and 120 h). The slope of each line was calculated by linear regression ($r^2 > 0.99$), and the water vapor transmission rate (*WVTR*) was measured from the slope of the straight line ($g\,h^{-1}$) by the test area (m^2). All values correlated to *WVTR* were corrected for the effect of gradient of concentration established in the stagnant air gap inside the cup, as seen on Eq. (4) (Gennadios, Weller, & Gooding, 1994):

$$WVPR_C = WVTR\left[\frac{(p_{w0} - p_{w2})}{(p_{w1} - p_{w2})}\right] \quad (4)$$

In which *WVTR* is the measured water vapor transmission rate ($g\,m^{-2}\,h^{-1}$); p_{w0} is the partial pressure of water vapor in air at the surface of distilled water (Pa), and p_{w1} is the partial water vapor pressure on the underside of film (Pa). As well as p_{w2} is the partial water vapor pressure of at the film surface outside the cup (Pa). Subsequently to the permeation tests, *WVP* ($g\,mm\,m^{-2}\,h^{-1}\,Pa^{-1}$) was calculated using Eq. (5):

$$WVP = \frac{WVPR_C \times L}{\Delta_P} \quad (5)$$

As it reads, $WVTR_c$ is the corrected water vapor transmission rate ($g\,m^{-2}\,h^{-1}$), L is the average film thickness (mm), and Δ_p is water vapor pressure difference between dry atmosphere and pure water.

2.2.12. Ex vivo *bioadhesion test*

The mucoadhesion of control and nanocomposite films was evaluated in a TA-XT2 Texture Analyzer (Stable Micro Systems). Fresh porcine colonic mucosa sections (4 cm^2) were placed on a support for mucoadhesion test, and films were also carefully attached to a cylindrical probe (10 mm), using double-sided tape. The probe was moved down at a constant speed of 10 $mm\,min^{-1}$ until it achieved predetermined compression force (0.5 N). To ensure the contact with the mucosa, the sample was introduced (1 mm deep) into the mucosal surface and kept for 60 s without force application during the contact phase. Then, the probe was moved up at a speed of 20 $mm\,min^{-1}$ and mucoadhesion force (F_{MA}) corresponding to the detachment maximum force (N) was measured. The work of the mucoadhesion (W_{MA}) (N s), provided by *AUC* of the force *versus* time curve, was determined for each sample. Prior to analysis, the films were pre-hydrated with phosphate buffer at colonic pH (pH 6.8), at 37 °C for 1 min.

2.2.13. MTX loading

Four milliliters of a MTX solution (25 $mg\,mL^{-1}$) was dripped to the nanocomposite films surface until complete absorption. Next, MTX-loaded nanocomposite films were dried in an oven with forced air circulation at 25 °C until they achieved constant weight.

2.2.14. In vitro *MTX release study*

RS/P-0.5CNF, RS/P-1.0CNF, RS/P-1.0BCN, RS/P-2.0BCN and RS/P-3.0BCN samples were selected for drug release tests based on their promising mucoadhesive properties. MTX-loaded RS/P films were also assayed as control. Dissolution tests were performed on a Hanson Research dissolution station (New Hanson SR-8 Plus) equipped with a paddle over the disk apparatus (USP V) (USP, 2007), according to sink conditions. The films were carefully fixed on the transdermal patch holder and placed in the bottom of vessels containing 900 mL of 0.1 mol/L phosphate buffer at colonic pH (pH 6.8), stirred at 50 rpm and equilibrated at 37 °C. Aliquots of 2 mL were withdrawn in predetermined intervals (15, 30, 45, 60, 90, 120, 150 and 180 min) and replaced by fresh medium at the same temperature. Samples were filtered through a 0.45 μm nylon filter prior to analysis. The MTX concentration was quantified by measuring the absorbance at 303 nm. MTX raw powder was tested as control.

3. Results and discussion

3.1. Macroscopic properties and thickness

CNF and BCN-RS/P nanocomposites were obtained as free-standing flexible films, macroscopically homogeneous, transparent and bubbles/fissures-free, as shown in Fig. 1B–C. The nanocomposite films prepared with higher cellulose nanofibers concentration were thicker, since after the water evaporation a higher polymer mass was deposited on the Petri dish. Therefore, in general, the thickness is proportional to the polymeric concentration (Bertuzzi, Vidaurre, Armada, & Gottifredi, 2007; Meneguin et al., 2014).

Likewise, the control film was significantly thinner than nanocomposite films ($p < 0.05$) due to the absence of nanocellulose that resulted in lower polymer mass. Thus, the thickness gradient of all films ranged between 0.055 and 0.188 mm.

3.2. Field emission gum scanning electron microscopy (FEG-SEM)

Micrographs analysis revealed films coating with different surfaces morphology, according to the type of reinforcement added, which suggests that CNF and BCN originated different patterns of interaction with the matrix.

RS/P-BCN nanocomposite films (Fig. 2A–D show the cellulose nanofibers presence covering the entire surface of the samples, which promotes an increased entanglement degree, as the BCN concentration raises, making the sample RS/P-3.0BCN denser. On the other hand, RS/P-CNF samples (Fig. 2E-H) showed a rough surface and the existence of tortuous structures. However, the presence of nanofibers on its surface was not observed, which might be an indicative of homogeneous dispersion of the phases. Lu, Weng, and Cao (2005) already reported the chemical compatibility between CNF and starch, possibly due to the establishment of strong hydrogen bonds occurring between these polymers.

The cross sections of control (Fig. 2Q) and nanocomposite films (Fig. 2I–P) indicate a change in the morphology promoted by reinforcement addition. The dense structure was preserved in nanocomposite films and no cracks or pores were observed, but the co-existence of two intercalated materials (RS/P and BCN or CNF) was evident (Fig. 2O).

3.3. FTIR spectroscopy

FTIR spectra of pectin, resistant starch, BCN, CNF, RS/P-3.0BCN and RS/P-3.0CNF are shown in Fig. 3. The main bands observed for isolated polymers (Fig. 3a–d) can be attributed to O—H stretching vibration (3500–3200 cm^{-1}), C—H stretching of the CH_2 and CH_3 groups (2908 cm^{-1}), along with the 1588 cm^{-1} band related to the bending vibrations of O—H. In the region of 1200–900 cm^{-1} several bands correspond to the C—O and C—C vibration bands of glycosidic bonds and pyranoid rings characteristic of the polysaccharides

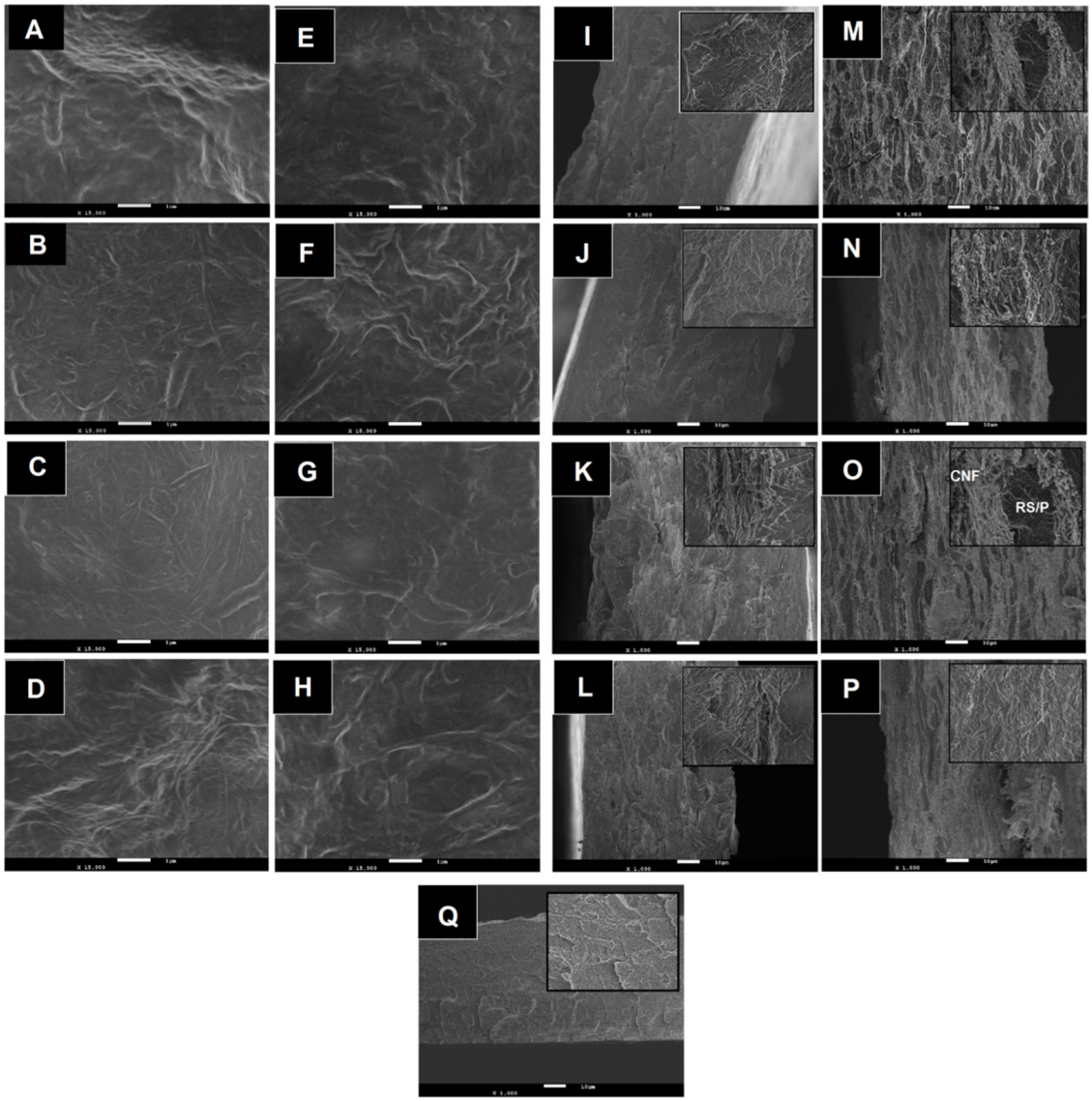

Fig. 2. FEG-SEM images (upper surface) taken at the same magnification (bar – 1 μm) of the samples: (A) RS/P-0.5BCN, (B) RS/P-1.0BCN, (C) RS/P-2.0BCN, (D) RS/P-3.0BCN, (E) RS/P-0.5CNF, (F) RS/P-1.0CNF, (G) RS/P-2.0CNF, and (H) RS/P-3.0CNF. Cross-sections were taken at 1000× and those recorded at 15,000 x magnification are embedded into the right-hand corner: (I) RS/P-0.5BCN, (J) RS/P-1.0BCN, (K) RS/P-2.0BCN, (L) RS/P-3.0BCN, (M) RS/P-0.5CNF, (N) RS/P-1.0CNF, (O) RS/P-2.0CNF, (P) RS/P-3.0CNF and (Q) RS/P films (control sample).

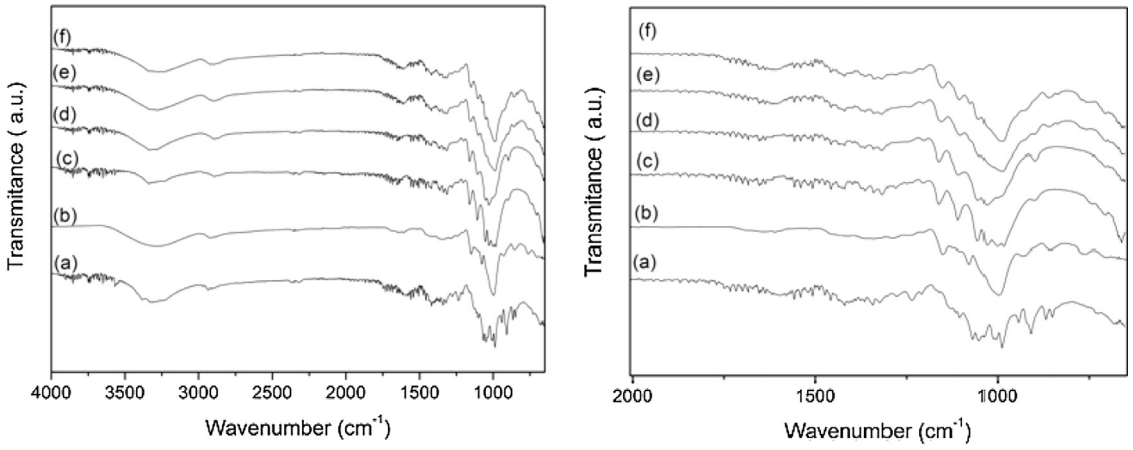

Fig. 3. FTIR spectra of: (a) pectin, (b) resistant starch, (c) BCN, (d) CNF, (e) RS/P-3.0BCN and (f) RS/P-3.0CNF.

structure (Barud et al., 2011; Nayak & Pal, 2013; Vityazev et al., 2017).

Despite the great similarity among the natural polysaccharides spectra, pectin spectrum (Fig. 3a) shows an additional band at 1720 cm^{-1} assigned to the C=O stretching vibration of methyl esterified carboxylic group in C6 position (Vityazev et al., 2017). RS (Fig. 3b) also exhibits a broader band in the region of 1200–900 cm^{-1}. Moreover, some band shifts in the spectrum of BCN (Fig. 3c) and CNF (Fig. 3d) were noted and related to the inter- and intramolecular interactions.

For RS/P-3.0BCN and RS/*P*-3.0CNF nanocomposite films (Fig. 3e,f), it was not observed significant vibrational changes, so that FTIR spectra represents only the sum of the individual polymers bands.

3.4. TG/DTG

TG/DTG curves of control and nanocomposite films were plotted in Fig. 4. Generally, the samples showed very similar behavior, with three to five weight loss events. All samples had a first discrete mass loss event around 6.2–10.9%, represented by a small broad peak on the DTG curve between 50 and 150 °C, which can be attributed to water desorption during the heating process, as it has been reported in polysaccharides studies (Soares, Castro, Cury, & Evangelista, 2013).

The second and main degradation stage (53.9–59.3%) occurred in a temperature range between 150 and 400 °C. The control film (RS/P) (Fig. 4a) exhibited in the DTG curve the appearance of two major events, the first one occurring at about 240 °C and related to the depolymerisation of pectin chains (Shi & Gunasekaran, 2008) and the second one at 280 °C attributed to the HAS degradation (Carbinatto, Castro, Cury, Magalhães, & Evangelista, 2012; Massicotte, Baille, & Mateescu, 2008). From this event is observed a continuous mass loss until 430 °C, when it occurs more two degradation stages with maximum decomposition (t_{onset}) at 435 (6.2%) and 526 °C (2.9%), respectively. These last two thermal events, represented by very narrow and intense peaks on the DTG curve, can be related to the degradation of the more ordered and crystalline fraction of the RS type III, represented by crystalline double helices stabilized by hydrogen bonds and structured in a three-dimensional way of high thermal stability (Eerlingen & Delcour, 1995).

TG curves obtained for RS/P-0.5BCN (Fig. 4b) and RS/P-0.5CNF (Fig. 4f) nanocomposites display very similar events of mass loss to control films, possibly due to the presence of BCN or CNF at a low amount (0.5%). However, the concentration increase of these compounds from 1.0 to 3.0% led to the disappearance of important thermal degradation events between 430 and 535 °C, which correspond to the more crystalline RS portions. This feature indicates a strong interaction between matrix and reinforcement phases, promoting the improvement of thermal stability. Furthermore, nanocomposite films obtained with higher amounts of reinforcement (RS/P-2.0BCN, RS/*P*-3.0BCN, RS/P-2.0CNF, RS/P-3.0CNF) had an additional event of mass loss in the range of 150–400 °C, which occurred at approximately 327, 330, 285, 288 and 322 °C, respectively. These thermal events happen due to the degradation of nanocellulose and it is mainly related to the depolymerization and decomposition of dehidrocelulose (Barud et al., 2015).

TG curves of the nanocomposite films containing the highest amounts of CNF (Fig. 4g-i) showed a discrete event between 190 and 210 °C that indicates the heterogeneous decomposition of CNF. This event was also observed by Aydemir (2015) for epoxy nanocomposites reinforced with cellulose nanofibrils.

3.5. XRD

Fig. 5 displays the XRD patterns of pectin, HAS, control film (RS/P), RS/P-3.0BCN and RS/P-3.0CNF representative nanocomposite films, which were chosen because of the similarity among XRD patterns of samples, regardless of the reinforcement concentration. Pectin exhibited intense peaks at 12.7, 16.72, 18.42, 25.32 and 40.14° (2θ), demonstrating its high crystallinity.

Starch is a complex semi-crystalline polymer composed by glucose polymers, namely amylose (linear portion) and amylopectin (branched portion), and presents different diffraction patterns, which depend on the water presence, length of amylopectin chains and packing density within granules (Sajilata, Singhal, & Kulkarni, 2006).

A, B and C patterns are representative of double helices with amylopectin of chain lengths of 23 to 29, 30–44 and 26–29 glucose units, respectively. According to Karim, Norziah, & Seow (2000), A-type pattern is exhibited by the cereal starches, B-type is displayed by tubers, fruits, high amylose maize and retrograded starch, while C-type pattern is intermediate of A and B types, observed in legume seed starches. Unlike, V polymorph assembles the structure in a simple helix assigned to amylose-lipid complexes (Warren, Gidley, & Flanagan, 2016; Mikus et al., 1946).

HAS (HYLON VII), a modified starch (70% amylose), depicted well-defined peaks of B-polymorph at 17.02, 19.8, 23 and 25° (2θ) (Carbinatto et al., 2012). The highest intensity of the peak happened around 19° (2θ), which suggests a highly ordered crystalline structure of amylose-lipid complexes in starch granules (Freire, Fertig, Podczeck, Veiga, & Sousa, 2009).

According to Lima et al. (2015) and also Kumar, Negi, Veena, and Bhardwaj (2014), BC membranes exhibit peaks at 14.8° and 16.1° (2θ) for (10$\bar{1}$) and (110) planes and other at 22.5° and 34.6° (2θ) for (200) and (004) planes. Additionally, they exhibit characteristics of type I native cellulose, while the XRD pattern of CNF has peaks at 16.7, 22.6 and 34.6° (2θ) assigned to diffraction planes (10$\bar{1}$), (002) and (040), respectively (Kaushik & Singh, 2011).

In control films (RS/P) diffractogram, it was observed the presence of new peaks at 13 and 21° (2θ), related to the changes in structural conformation and the presence of V-polymorph, which are an efficiency indicative on the starch retrogradation process. In addition, a broad peak is noticed at 16.5° (2θ), and it was assigned to the pectin presence (Htoon et al., 2010; Meneguin et al., 2014).

XRD patterns of RS/P-3.0CNF showed a broad peak at about 16° (2θ), which indicates the presence of overlapped cellulose, pectin, and RS patterns, while diffraction peaks at 22.5 and 34.2° (2θ) are related to the CNF. However, the RS/P-3.0BCN diffractogram depicted additional peaks at 14.6, 17.01 and 19.8° (2θ), attributed to BC and HAS, information that confirms the blend obtainment.

3.6. Mechanical properties of composite films

Films coating should present suitable mechanical resistance to support processing, packing, storage and transport, ensuring the effectiveness of coating processes, as well as avoiding the formation of pores and fissures on the surface, which can accelerate degradation and drugs release events, and facilitating instability reactions (Felton, 2007). Nanocelluloses act as an excellent mechanical reinforcement due to their fibers alignment and orientation, giving rise to a more resistant material that supports large fracture forces before the yield point is reached (Aitomäki & Oksman, 2014).

The effect of BCN or CNF addition at different concentrations on mechanical properties of nanocomposite films is presented at Table 1. It revealed the development of materials with improved strength in comparison to control samples, which can be related to the intrinsic rigidity of nanofibrils and the homogeneous dispersion of their phases.

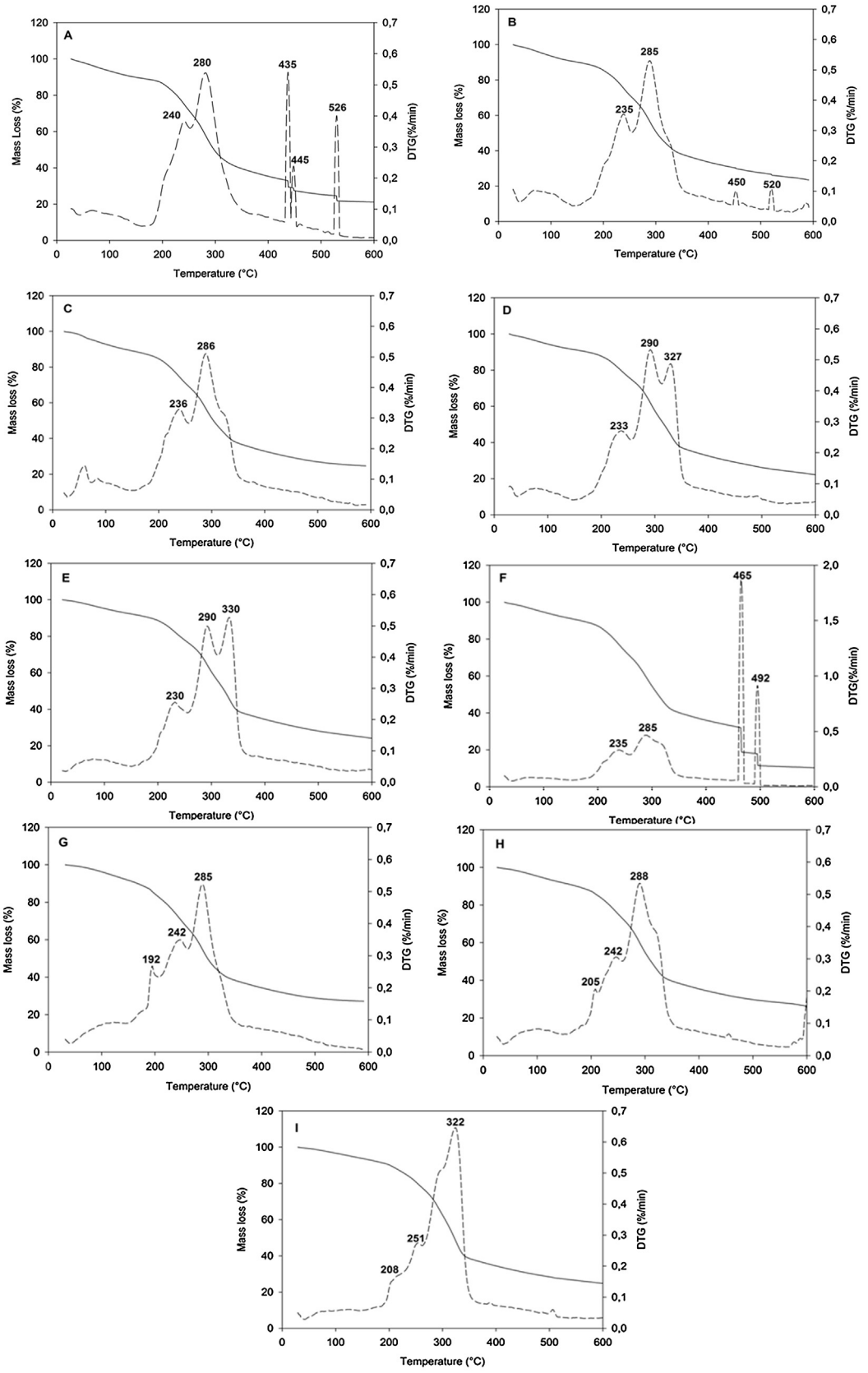

Fig. 4. TG/DTG curves: (a) RS/P control film, (b) RS/P-0.5BCN, (c) RS/P-1.0BCN, (d) RS/P-2.0BCN, (e) RS/P-3.0BCN, (f) RS/P-0.5CNF, (g) RS/P-1.0CNF, (h) RS/P-2.0CNF and (i) RS/P-3.0CNF.

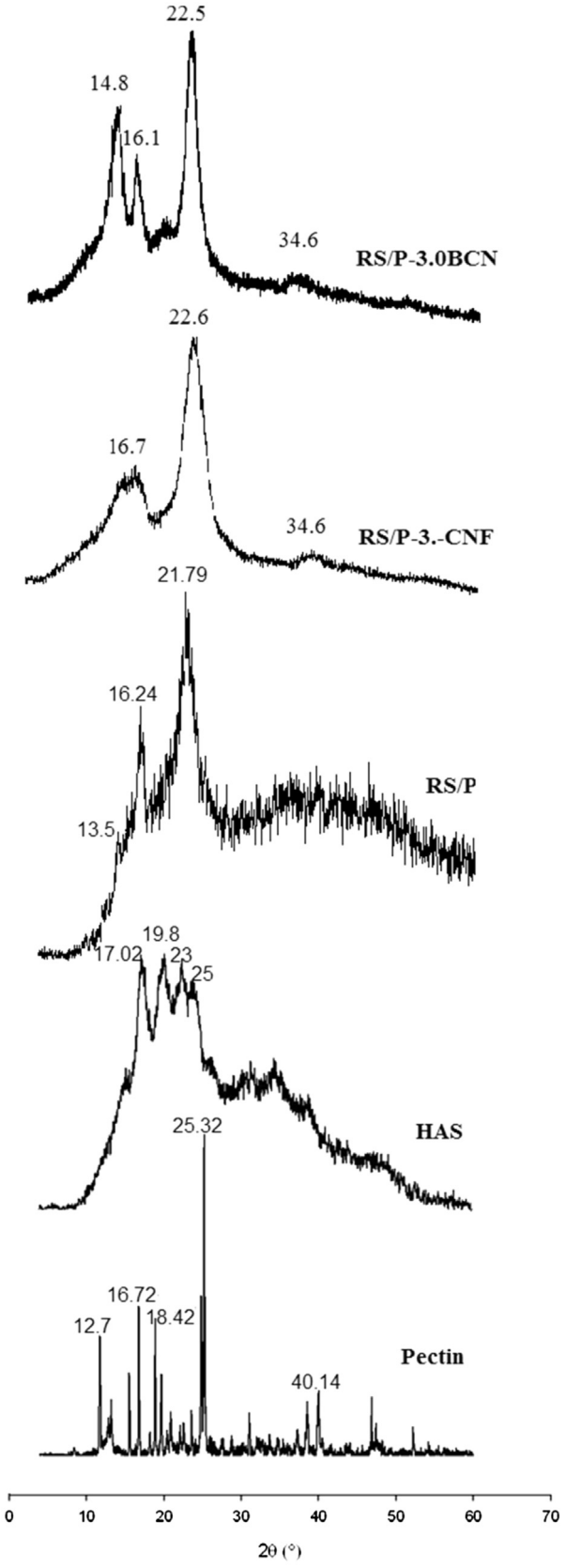

Fig. 5. X-ray diffraction patterns of the pectin, HAS, control (RS/P) and representative nanocomposite films (RS/P-3.0BCN and RS/P-3.0CNF).

Table 1
Mechanical properties of control and nanocomposites films (mean ± SD, $n = 5$).

Samples	P_s (MPa)	E_b (%)	E_p (kJ m^{-3})
RS/P-0.5BCN	13.64 ± 2.54	5.68 ± 1.13	8.99 ± 1.74
RS/P-1.0BCN	13.69 ± 4.32	2.43 ± 1.36	3.23 ± 1.37
RS/P-2.0BCN	16.81 ± 2.83	4.75 ± 0.96	5.75 ± 1.02
RS/P-3.0BCN	13.29 ± 1.77	5.29 ± 2.31	2.98 ± 0.95
RS/P-0.5CNF	8.03 ± 3.40	3.32 ± 1.46	1.08 ± 0.01
RS/P-1.0CNF	21.92 ± 3.21	5.23 ± 1.50	6.52 ± 1.49
RS/P-2.0CNF	15.65 ± 1.76	8.84 ± 3.13	5.88 ± 1.96
RS/P-3.0CNF	24.32 ± 2.35	5.61 ± 1.05	5.35 ± 1.55
RS/P	9.54 ± 1.27	0.96 ± 0.01	0.29 ± 0.05

Despite the increase in BCN concentration at RS/P-BCN nanocomposites did not have led to the increment of *Ps* values ($p > 0.05$), it was found that RS/P-0.5BCN required a E_p (8.9 kJ m^{-3}) that was about three times greater than RS/P-1.0BCN (3.2 kJ m^{-3}) and RS/P-3.0BCN (2.9 kJ m^{-3}) samples. Such information suggests that the lower BCN concentration is responsible for building less packaged structures, but it also allows greater polymeric chains mobility when a force is applied (Felton, 2007).

On the other hand, the construction of a sufficiently compacted polymeric network to better withstand the applied force, at the same time with adequate flexibility not to become brittle, assured to RS/P-2.0BCN film higher P_s (16.8 MPa) values than to control films (9.5 MPa) ($p < 0.05$). According to Dayal and Catchmark (2016), another key factor in the composites mechanical properties is in the difficulty in which water bound to matrix/reinforcement leaves the polymeric structure during force application. In other words, for RS/P-2.0BCN sample, a high degree of interaction between RS/P and BCN may have been established and they were able to withstand a water outlet, preserving the polymer network and reflecting a greater resistance.

Nevertheless, the CNF addition to the nanocomposites was more efficient, resulting in more resistant films to the perforation in relation to control samples ($p < 0.05$) (exception RS/P-0.5CNF). It was reached P_s values up to 24.3 MPa for RS/P-3.0CNF, which should be related to the less porous network of CNF in comparison to BCN network, which results in a more effective strength (Aitomäki & Oksman, 2014). In addition, the reduced interstitial spaces must be more easily filled, occupying the void spaces without leading it to an increase of free volume and creating an entangled cellulosic network. However, RS/P-1.0CNF, RS/P-2.0CNF and RS/P-3.0CNF samples presented similar P_s ($p > 0.05$), meaning that low amounts of CNF are enough to make films more resistant.

It is important to notice that mechanical properties of composites containing nanocellulose are also related to strong interactions *via* hydrogen bonds which occur in large quantities. Crystalline and amorphous portions of nanocellulose, related to the structured and unstructured phases, also play an important role to elevate mechanical strength, since the first portion is responsible for the rigidity and the another for flexibility (Lin & Dufresne, 2014).

The raise of BCN and CNF concentration at nanocomposite films did not lead to the improvement of elongation at break (E_b) ($p > 0.05$) (except for RS/P-0.5CNF and RS/P-2.0CNF), but RS/P-0.5BCN (5.6%), RS/P-3.0BCN (5.2%), RS/P-1.0CNF (5.2%), RS/P-2.0CNF (8.8%) and RS/P-3.0CNF (5.6%) samples showed higher E_b values than those found in control samples (0.96%) ($p < 0.05$). They reached E_b values from 5.4 to 9.3 times higher, which clearly indicates that the microstructure of nanocomposite films is able to rearrange itself with the load application in a more flexible cellulosic array.

3.7. *Water vapor permeability (*WVP)

The *WVP* study has been considered as an important tool to check barrier properties that films coating offer against humidity

Table 2
Water vapor permeability (*WVP*), mucoadhesive force (F_{MA}) (N) and mucoadhesion work (W_{MA}) (N.s) of control and nanocomposite films (mean ± SD, $n = 6$).

Samples	*WVP* ($\times 10^{-5}$ g mm m^{-2} h^{-1} Pa^{-1})	F_{MA} (N)	W_{MA} (N s)
RS/P-0.5BCN	3.95 ± 0.14	2.82 ± 0.86	2.53 ± 0.45
RS/P-1.0BCN	3.27 ± 0.38	5.37 ± 0.95	4.85 ± 2.27
RS/P-2.0BCN	4.01 ± 0.28	8.88 ± 0.67	8.83 ± 0.84
RS/P-3.0BCN	4.65 ± 0.16	9.25 ± 1.28	6.52 ± 2.46
RS/P-0.5CNF	4.57 ± 0.11	8.27 ± 3.08	12.26 ± 2.47
RS/P-1.0CNF	4.61 ± 0.63	12.46 ± 2.55	11.49 ± 3.09
RS/P-2.0CNF	4.85 ± 0.24	4.80 ± 1.56	3.25 ± 0.31
RS/P-3.0CNF	3.50 ± 0.18	3.61 ± 0.83	4.09 ± 1.14
RS/P	19.10 ± 4.06	1.14 ± 0.06	1.01 ± 0.11

penetration, allowing a better understanding of polymeric interactions type involved in the polymeric matrix and its hydrophilicity (Akhagari, Farahmand, Garekani, Sadeghi, & Vandamme, 2006; Meneguin et al., 2014).

Considering the results presented on Table 2, it was verified that nanocomposite films show excellent barrier properties in relation to control films ($p < 0.05$), since the permeability to water molecules through their structures was between 3.9 and 5.8 times lower, confirming the filling effect exerted by BCN or CNF addition. This behavior is consistent alongside the findings on FEG-SEM images, in which the nanocelluloses addition was responsible for building tortuous paths in the matrix, which are responsible for hindering the water molecules diffusion (Oliveira et al., 2015; Shahmohammadi & Almasi, 2016). Moreover, the reduced *WVP* values may be related to the hydrophilicity decrease of the nanocomposite films, resulting in overcoming of some drawbacks, such as the high water solubility of the previous RS/P films (Meneguin et al., 2014), which should be further confirmed by swelling and solubility test.

Despite the difference in thickness among the nanocomposite films, as well as different concentrations and types of nanocelluloses used as reinforcement, no significant differences among nanocomposites WVP were observed ($p > 0.05$).

3.8. Ex-vivo *mucoadhesion test*

The great interest in the development of mucoadhesive systems lies in the fact that they provide a possible increase of bioavailability, which means that the use of reduced doses of drugs achieves the same therapeutic effect. Besides, it reduces the side effects occurrence, and finally, it contributes to reduce its cost. Interestingly, these systems also allow targeting the drug to specific organs and/or tissues using specific polymers as stimuli-sensitive polymers (or smart polymers) (Ameye et al., 2002; Andrews, Laverty, & Jones, 2009).

The parameters evaluated in this test were both mucoadhesion force (F_{MA}) and mucoadhesion work (W_{MA}), which are summarized in Table 2. The first one corresponds to the maximum detachment force between the analytical probe and the porcine colonic mucosa, and the second one is related to the detachment energy.

The F_{MA} of films obtained through BCN addition ranged from 2.8 to 9.2 N, suggesting the establishment of an important mucoadhesion process. The comparison among the samples prepared with BCN showed that the increase in the load concentration from 0.5 to 3.0% led to a raise of F_{MA} (about 3.2%) ($p < 0.05$), which probably is related to the existence of a greater number of functional groups in the polymeric chains that interact with mucin (Wittaya-Areekul, Kruenate, & Prahsarn, 2006). Moreover, increasing concentrations of hydrophilic polymers are generally associated with increased swellability, which has great influence during the establishment of mucoadhesive process. This is due to a viscous surface formation, which will spread on the mucin layer, according to the wettability theory (Dodou, Breedveld, & Wieringa, 2005).

RS/P-1.0CNF film exercised the highest interaction with a biological membrane (about 12.45 N). However, above this concentration, it was observed that F_{MA} decreased and this behavior can be related to the construction of denser structures (Barud et al., 2015), hindering the process of interpenetration in mucin chains, since the system must be flexible enough to interpenetrate in mucus layers (Andrews et al., 2009).

Finally, W_{MA} results are in agreement with the F_{MA}, meaning that the samples had a greater mucoadhesive force required an higher mucoadhesion work.

In relation to the high potential mucoadhesive of nanocomposite films, it is expected that some intrinsic features of the GIT will contribute to the mucoadhesion occur specifically in the colonic environment. The pH-triggered mucoadhesion must occur because these materials were developed from anionic polymers that have their carboxyl groups protonated when in contact with gastric medium (pH 1.2), maintaining the polymer chains more rigid and entangled. Unlike, the raised pH (pH 6.8) in the colonic portion causes the ionization of the COOH groups to COO–, promoting the repulsion of the polymer chains, which become more flexible and able to interact with the mucin chains.

The fastest mucus turnover rate in stomach and small intestine contributes to the non-adhesion of dosage forms in the GIT upper portions (Davis, 2005). According to Varum, Basit, Sousa, and Veiga (2008), it has been verified a great failure in mucoadhesive process from upper portions of GIT, revealing the colon as an ideal organ for the establishment of mucoadhesion based on its slowest mucus turnover rate, longer transit time and the thicker mucus layer.

3.9. In vitro *MTX release*

Dissolution profiles of MTX from control and nanocomposite films, as well as the raw material were evaluated in 0.1 mol/L phosphate buffer (pH 6.8) in order to simulate the colonic pH, and are presented on Fig. 6. About 30% of raw MTX was released in the first 15 min of test and the $t_{80\%}$ (time required to release 80% of drug) was 210 min. The highest MTX release rates from nanocomposite films were observed with a burst release ranging from 40.84 to 64.13% (up to two times higher than free MTX), in the first 15 min of test. Such data indicates that developped films were able to increase the MTX release, which constitutes an important strategy to overcome oral bioavailability problems of poorly soluble drugs.

The enhancement in MTX release rates in colonic pH (6.8) reveals the influence of the nanofibrils nanometric size in the release accelaration, regarding the large surface area and the short diffusion path, as expressed by the Noyes-Whitney equation (Noyes & Whitney, 1897). Moreover, this behavior is associated to intrinsic BCN and CNF characteristics, such as the high crystallinity, swellability, hydrophilicity, as well as their porous structure, which together facilitate the drug diffusion through the polymer matrix (Shahmohammadi & Almasi, 2016; Valo et al., 2011).

It is important to notice that different amounts of MTX were released in the first 15 min from samples obtained with various BCN or CNF loads. The lowest MTX release (%) was attributed to the RS/P-0.5CNF (40.84%), as opposed to about 55, 48, 53 and 54% for RS/P-1.0CNF, RS/P-1.0BCN, RS/P-2.0BCN and RS/P-3.0BCN, respectively, highlighting the highest release rates from RS/P control film (64.13%) ($p < 0.05$). The better control of release rates from RS/P-0.5CNF can be attributed to the less porous structure of CNF in relation to BCN (Aitomäki & Oksman, 2014). Whereas the nanofiller absence, with a less physically crosslinked polymeric network, probably led to a MTX release rates acceleration in the RS/P con-

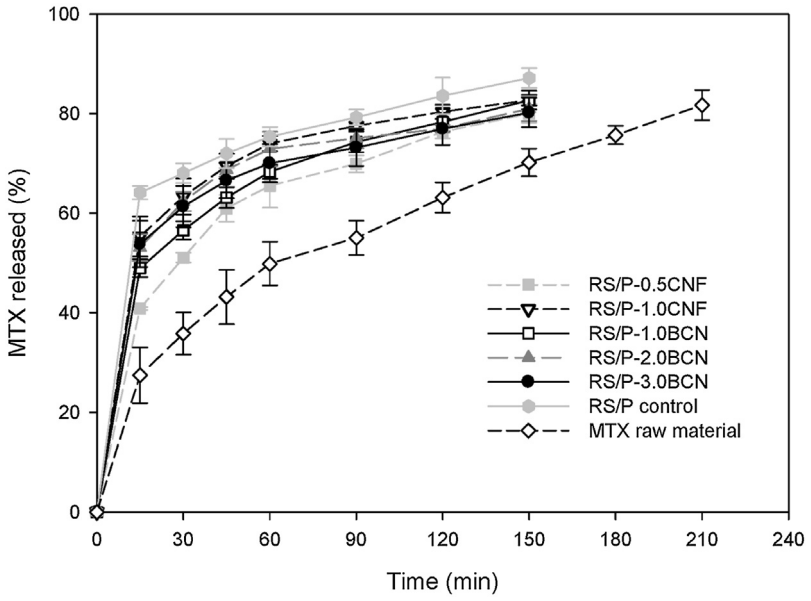

Fig. 6. *In vitro* MTX release profiles from control, nanocomposite films and MTX raw material in phosphate buffer (pH 6.8).

trol film, which presented visible degradation after the test, while nanocomposites films were still intact.

4. Conclusions

In a previous work, the promising properties of RS/P films as a potential strategy for colon-specific drug delivery was already verified. Now, these films were reinforced with different types of nanocellulose by a simple process, with low costs and green, *i.e.* without the use of organic solvents and crosslinker agents. The correlation between the results of the mechanical tests, mucoadhesion and MTX release indicates that plant cellulose nanofibers (CNF) obtained by grinder are the best nanofiller. This probably happens because there is the presence of fibers only at nanoscale due to the efficiency of the defibrillation method (grinder). Meanwhile, for those fibers obtained from the BC membranes (BCN) through the high-energy homogenizer, nano and micro-scale can coexist in the same material, producing a pattern of weaker interaction along the matrix.

These results alongside with the improvement of MTX release rates in colonic pH confirm the potential of nanocomposites films developed as an important technologic platform for specific pharmaceutical needs, such as the enhancement of oral bioavailability of poorly water-soluble drugs as well as to design colon-specific drug delivery systems. In addition, anatomic-physiologic differences throughout the various portions of GIT should contribute technologically as trigger-mechanism of the mucoadhesion at a target organ. Thus, it is expected that physiological factors such as pH, mucus layer thickness and transit time of the colon contribute to the mucoadhesion of developed nanocomposite films, also favoring the MTX colon-specific release.

Acknowledgements

The financial support provided by Coordenação de Aperfeiçoamento de Pessoal de Nivel Superior (CAPES) and Fundação de Amparo à Pesquisa do Estado de Sao Paulo (FAPESP) is acknowledged. We would like to dedicate this work to the memory of our dear Professor Raul Cesar Evangelista.

References

Abeer, M. M., Iqbal, M. C., & Martin, C. (2014). A review of bacterial cellulose-based drug delivery systems: Their biochemistry, current approaches and future prospects. *Journal of Pharmacy and Pharmacology*, *66*, 1047–1061.
Aitomäki, Y., & Oksman, K. (2014). Reinforcing efficiency of nanocellulose in polymers. *Reactive and Functional Polymers*, *85*, 151–156.
Akhagari, A., Farahmand, F., Garekani, H. A., Sadeghi, F., & Vandamme, T. F. (2006). Permeability and swelling studies on free films containing insulin in combination with different polymethacrylates aimed for colonic drug delivery. *European Journal of Pharmaceutical Science*, *28*, 307–314.
Ameye, D., Voorspoels, J., Foreman, P., Tsai, J., Richardson, P., Geresh, S., et al. (2002). Ex vivo bioadhesion and in vivo testosterone bioavailability study of different bioadhesive formulations based on starch-g-poly(acrylic acid) copolymers and starch/poly(acrylic acid) mixtures. *Journal of Controlled Release*, *79*, 173–182.
Andrews, G. P., Laverty, T. P., & Jones, D. S. (2009). Mucoadhesive polymeric platforms for controlled drug delivery. *European Journal of Pharmaceutics and Biopharmaceutics*, *71*, 505–518.
Aydemir, D. (2015). Morphological and thermal properties of cellulose nanofibrils reinforced epoxy nanocomposites. *DRVNA Industrija*, *66*, 35–40.
Barud, H. S., Souza, J. L., Santos, D. B., Crespi, M. S., Ribeiro, C. A., Messaddeq, Y., et al. (2011). Bacterial cellulose/poly(3-hydroxybutyrate) composite membranes. *Carbohydrate Polymers*, *83*, 1279–1284.
Barud, H. G. O., Barud, H. S., Cavicchioli, M., Amaral, T. S., Oliveira, O. B., Jr, Santos, D. M., et al. (2015). Preparation and characterization of a bacterial cellulose/silk fibroin scaffold for tissue regeneration. *Carbohydrate Polymers*, *128*, 41–51.
Bertuzzi, M. A., Vidaurre, E. F. C., Armada, M., & Gottifredi, J. C. (2007). Water vapor permeability of edible starch based films. *Journal of Food Engineering*, *80*, 972–978.
Carbinatto, F. M., Castro, A. D., Cury, B. S. F., Magalhães, A., & Evangelista, R. C. (2012). Physical properties of pectin–high amylose starch mixtures cross-linked with sodium trimetaphosphate. *International Journal of Pharmaceutics*, *423*, 281–288.
Cury, B. S. F., Meneguin, A. B., Cardoso, V. M. O., & Prezotti, F. G. (2014). Oral drug release systems based on pectin. In P. L. Bush (Ed.), *Pectin: Chemical properties, uses and health benefits* (pp. 65–81). New York: Nova Science Publishers.
Davis, S. S. (2005). Formulation strategies for absorption windows. *Drug Discovery Today*, *10*, 249–257.
Dayal, M. S., & Catchmark, J. M. (2016). Mechanical and structural property analysis of bacterial cellulose composites. *Carbohydrate Polymers*, *144*, 447–453.
Dodou, D., Breedveld, O., & Wieringa, P. A. (2005). Mucoadhesives in the gastrointestinal tract: Revisiting the literature for novel applications. *European Journal of Pharmaceutics and Biopharmaceutics*, *60*, 1–16.
Eerlingen, R. C., & Delcour, J. A. (1995). Formation, analysis, structure and properties of type III enzyme resistant starch. *Journal of Cereal Science*, *22*, 129–138.
Eichhorn, S. J., Dufresne, A., Aranguren, M., Marcovich, N. E., Capadona, J., Rowan, S. J., et al. (2010). Review: Current international research into cellulose nanofibres and nanocomposites. *Journal of Materials Science*, *45*, 1–33.
Felton, L. A. (2007). Characterization of coating systems. *AAPS PharmSciTech*, *8*, E1–E9.

Freire, A. C., Fertig, C. C., Podczeck, F., Veiga, F., & Sousa, J. (2009). Starch-based coatings for colon-specific drug delivery. Part I: The influence of heat treatment on the physico-chemical properties of high amylose maize starches. *European Journal of Pharmaceutics and Biopharmaceutics*, *72*, 574–586.
Gennadios, A., Weller, C. L., & Gooding, C. H. (1994). Measurement errors in water vapor permeability of highly permeable, hydrophilic edible films. *Journal of Food Engineering*, *21*, 395–409.
He, W., Du, Q., Cao, D.-Y., Xiang, B., & Fan, L.-F. (2008). Study on colon-pecific pectin/ethylcellulose film-coated 5-fluorouracil pellets in rats. *International Journal of Pharmaceutics*, *348*, 35–45.
Htoon, A. K., Uthayakumaran, S., Piyasiri, U., Appelqvist, A. M., Lopez-Rubio, A., Gilbert, E. P., et al. (2010). The effect of acid dextrinisation on enzyme-resistant starch content in extruded maize starch. *Food Chemistry*, *120*, 140–149.
Jorfi, M., & Foster, E. J. (2015). Recent advances in nanocellulose for biomedical applications. *Journal of Applied Polymer Science*, *132*, 1–19.
Juncu, G., Stoica-Guzun, A., Stroescu, M., Isopencu, G., & Jinga, S. I. (2015). Drug release kinetics from carboxymethylcellulose-bacterial cellulose composite films. *International Journal of Pharmaceutics, Corrected Proof*, in press.
Karim, A. A. B. D., Norziah, M. H., & Seow, C. C. (2000). Methods for the study of starch retrogradation. *Food Chemistry*, *71*, 9–36.
Kaushik, A., & Singh, M. (2011). Isolation and characterization of cellulose nanofibrils form wheat straw using explosion coupled with high shear homogenization. *Carbohydrate Research*, *346*, 76–85.
Kim, J.-H., Shim, B. S., Kim, H. S., Lee, Y.-J., Min, S.-K., Jang, S., et al. (2015). Review of nanocellulose for sustainable future materials. *International Journal of Precision Engineering and Manufacturing-Green Technology*, *2*, 197–213.
Koetting, M. C., Guido, J. F., Gupta, M., Zhang, A., & Peppas, N. A. (2016). pH-responsive and enzymatically-responsive hydrogel microparticles for the oral delivery of therapeutic proteins: Effects of protein size, crosslinking density, and hydrogel degradation on protein delivery. *Journal of Controlled Release*, *221*, 18–25.
Kumar, A., Negi, S. Y., Veena, C., & Bhardwaj, N. K. (2014). Characterization of cellulose nanocrystals produced by acid-hydrolysis from sugarcane bagasse as agro-waste. *Journal of Materials Physics and Chemistry*, *1*, 1–8.
Lima, L. R., Santos, D. B., Santos, M. V., Barud, H. S., Henrique, M. A., Pasquini, D., et al. (2015). Nanocristais de celulose a partir de celulose bacteriana. *Química Nova*, *38*, 1140–1147.
Limmatvapirat, S., Limmatvapirat, C., Puttipipatkhachorn, S., Nuntanid, J., & Luangtana-Anan, M. (2007). Enhanced enteric properties and stability of shellac films through composite salts formation. *European Journal of Pharmaceutical and Biopharmaceutics*, *67*, 690–698.
Lin, N., & Dufresne, A. (2014). Nanocellulose in biomedicine: Current status and future prospect. *European Polymer Journal*, *59*, 302–325.
Liu, L., Fishman, M. L., Kost, J., & Hicks, K. B. (2003). Pectin-based systems for colon-specific drug delivery via oral route. *Biomaterials*, *24*, 3333–3343.
Lu, Y., Weng, L., & Cao, X. (2005). Biocomposites of plasticized starch reinforced with cellulose crystallites from cottonseed linter. *Macromolecular Bioscience*, *5*, 1101–1107.
Mandal, A., & Chakrabarty, D. (2015). Characterization of nanocellulose reinforced semi-interpenetrating polymer network of poly(vinyl alcohol) & polyacrylamide composite films. *Carbohydrate Polymers*, *134*, 240–250.
Massicotte, L. P., Baille, W. E., & Mateescu, M. A. (2008). Carboxylated high amylose starch as pharmaceutical excipient. Structural insights and formulation of pancreatic enzymes. *International Journal of Pharmaceutics*, *356*, 212–223.
Maurer, J. M., Hofman, S., Schellekens, R. C. A., Tonnis, W. F., Dubois, A. O. T., Woerdenbag, H. J., et al. (2016). Development and potential application of an oral ColoPulse infliximab tablet with colon specific release: A feasibility study. *International Journal of Pharmaceutics*, *505*, 175–186.
Meneguin, A. B., Cury, B. S. F., & Evangelista, R. C. (2014). Films from resistant starch-pectin dispersions intended for colonic drug delivery. *Carbohydrate Polymers*, *99*, 140–149.
Nayak, A. K., & Pal, D. (2013). Blends of jackfruit seed starch–pectin in the development of mucoadhesive beads containing metformin HCl. *International Journal of Biological Macromolecules*, *62*, 137–145.
Noyes, A., & Whitney, W. R. (1897). The rate of solution of solid substances in their own solutions. *Journal of the American Chemical Society*, *19*, 930–934.
Oliveira, R. L., Barud, H. S., De Salvi, D. T. B., Perotti, G. F., Ribeiro, S. J. L., & Constantino, V. R. L. (2015). Transparent organic–inorganic nanocomposites membranes based on carboxymethylcellulose and synthetic clay. *Industrial Crops and Products*, *69*, 415–423.
Qiao, K., Zheng, Y., Guo, S., Tan, J., Chen, X., Li, J., et al. (2015). Hydrophilic nanofiber of bacterial cellulose guided the changes in the micro-structure and mechanical properties of nf-BC/PVA composites hydrogels. *Composites Science and Technology*, *118*, 47–54.
Rhim, J.-W. (2011). Effect of clay contents on mechanical and water vapor barrier properties of agar-based nanocomposite films. *Carbohydrate Polymers*, *86*, 691–699.
Saha, N. R., Sarkar, G., Roy, I., Rana, D., Bhattacharyya, A., Adhikari, A., et al. (2016). Studies on methylcellulose/pectin/montmorillonite nanocomposite films and their application possibilities. *Carbohydrate Polymers*, *136*, 1218–1227.
Sajilata, M. G., Singhal, R. S., & Kulkarni, P. R. (2006). Resistant starch—A review. *Comprehensive Reviews in Food Science and Food Safety*, *5*, 1–17.
Shahmohammadi, F., & Almasi, H. (2016). Morphological, physical, antimicrobial and release properties of ZnO nanoparticles-loaded bacterial cellulose films. *Carbohydrate Polymers*, *149*.
Shi, L., & Gunasekaran, S. (2008). Preparation of pectin–ZnO nanocomposite. *Nano Express*, *3*, 491–495.
Soares, G. A., Castro, A. D., Cury, B. S. F., & Evangelista, R. C. (2013). Blends of cross-linked high amylose starch/pectin loaded with diclofenac. *Carbohydrate Polymers*, *91*, 135–142.
United States Pharmacopeia & National Formulary. (2007). *Rockville: United States pharmacopeial convention* (30th ed.). Easton: Mack.
Valo, H., Kovalainen, M., Laaksonen, P., Häkkinen, M., Auriola, S., Peltonen, L., et al. (2011). Immobilization of protein-coated drug nanoparticles in nanofibrillar cellulose matrices-enhanced stability and release. *Journal of Controlled Release*, *156*, 390–397.
Varum, F. O., Basit, A. W., Sousa, J., & Veiga, F. (2008). Estudos de mucoadesão no trato gastrointestinal para o aumento da biodisponibilidade oral de fármacos. *Brazilian Journal of Pharmaceutical Sciences*, *44*, 535–548.
Vityazev, F. V., Fedyuneva, M. I., Golovchenko, V. V., Patova, O. A., Ipatova, E. U., Durnev, E. A., et al. (2017). Pectin-silica gels as matrices for controlled drug release in gastrointestinal tract. *Carbohydrate Polymers*, *157*, 9–20.
Warren, F. J., Gidley, M. J., & Flanagan, B. M. (2016). Infrared spectroscopy as a tool to characterise starch ordered structure—A joint FTIR-ATR, NMR, XRD and DSC study. *Carbohydrate Polymers*, *139*, 35–42.
Wittaya-Areekul, S., Kruenate, J., & Prahsarn, C. (2006). Preparation and in vitro evaluation of mucoadhesive properties of alginate/chitosan microparticles containing prednisolone. *Internation Journal of Pharmaceutics*, *312*, 113–118.